Chapter 4

Perovskite Quantum Dot Light-Emitting Diodes

Zhifeng Shi, Xinjian Li and Chongxin Shan

Additional information is available at the end of the chapter

http://dx.doi.org/10.5772/intechopen.68275

Abstract

Recently, lead halide perovskite quantum dots (QDs) have attracted much attention because of their excellent properties of high color purity, tunable emission wavelength covering the whole visible region, and ultrahigh photoluminescence (PL) quantum yield. They are expected to be promising candidates for the next-generation cost-effective lighting and display sources. Here, we introduced the recent development in the direct solution-processed synthesis and ion exchange-based reactions, leading to organic/inorganic hybrid halide perovskites ($CH_3NH_3PbX_3$; X = Cl, Br, I) and all-inorganic lead halide perovskites ($CsPbX_3$; X = Cl, Br, I), and studied their optical properties related to exciton-related emission and quantum confinement effect. Finally, we reviewed the recent progresses on the perovskite light-emitting diodes (LEDs) based on $CH_3NH_3PbX_3$ and $CsPbX_3$ quantum dots and provided a critical outlook into the existing and future challenges.

Keywords: perovskite, $CH_3NH_3PbX_3$, cesium lead halide, light-emitting diodes

1. Introduction

Motivated by the remarkable color tunability and relatively high photoluminescence (PL) quantum yield of colloidal quantum dots (QDs), the concepts of QD-based light-emitting diodes (LEDs) have been proposed and developed for a few years, and multicolor LEDs were successfully fabricated either for PL or electroluminescence (EL) mechanism [1–6]. It has been recognized that using QD-based LEDs as the backlighting system of liquid crystal display can greatly expand the color gamut of display and present vibrant colored images [7]. Although the conventional CdSe-based QD system has been commercially used, it suffers from the lack of surface control during process and low-cost preparation technique [8]. Moreover, development of high-performance CdSe QD-based LEDs strongly relies on the precise core/shell design, involving the band engineering and surface ligands. In this circumstance, colloidal lead halide perovskite QDs began to attract a great scientific attention. The appealing properties

of this new class of materials that might enable advances in electroluminescent devices are their outstanding optical properties including the narrow emission band (<20 nm), a wide wavelength tunability (400–800 nm), and a high PL quantum yield, which make them suitable for high-performance, low-cost, and lightweight LED applications [9–11]. Beyond LEDs, they were also explored as interesting materials for low-threshold lasing [12], photodetectors [13], and solar cells [14]. And, many studies on these fields have been reported recently. In the following, two typical synthesized methods for the novel perovskite QDs system were introduced in detail, and their optical properties related to the exciton-related emission and quantum confinement effect were investigated. Finally, we reviewed the previously reported device structures on perovskite QD LEDs and provided a critical outlook into the existing and future challenges.

2. Crystal structure features

Lead halide perovskite QDs have a crystal structure of ABX_3, in which A and B are the monovalent and divalent cations, respectively, and X is a monovalent halide anion (Cl, Br, I). The typical crystal structure of lead halide perovskites was illustrated in **Figure 1a**. B cation is coordinated to six halide ions in an octahedral configuration, and the octahedra are corner-sharing, with the A cation located in between those octahedra. In addition, the lead halide perovskite QDs can fall into two categories depending on the chemical component of A cation, organic-inorganic hybrid, and all-inorganic perovskites. Methylammonium (MA) lead trihalide perovskites have so far been the most intensively explored in optoelectronics, and they have the chemical composition of $MAPbX_mY_{3-m}$. This perovskite is a hybrid inorganic-organic direct-bandgap semiconductor. Also, the perovskites based on colloidal $CsPbX_3$ QDs are extensively investigated in recent years. As is well known, $MAPbX_3$ or $CsPbX_3$ QDs can crystalline in orthorhombic, tetragonal, and cubic polymorphs according to the environment temperature and total system energy. And, experimental results have confirmed that $MAPbX_3$ or $CsPbX_3$ QDs possess different crystal structures at different temperatures or with different halide ions [15]. For the

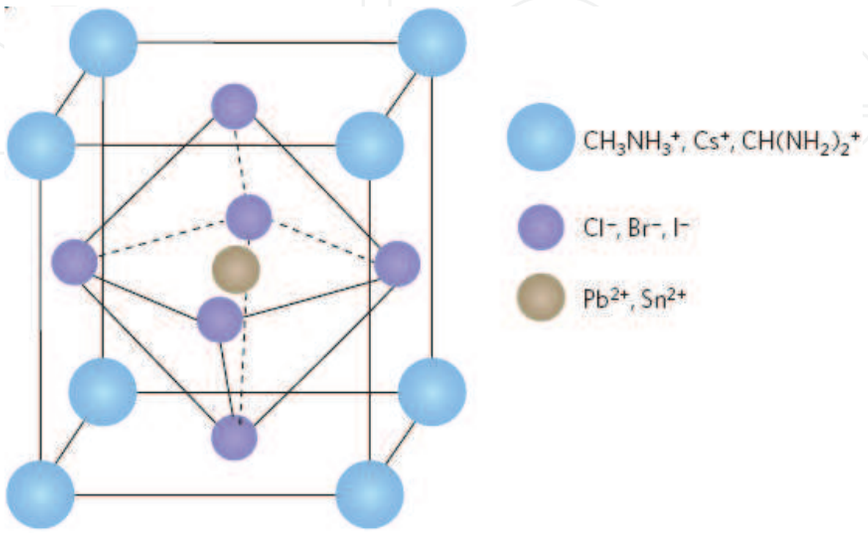

Figure 1. Illustration of the perovskite crystal structure.

two types of perovskite QDs, their optical and electronic properties are tunable by varying the composition of constituted halide ions and a smaller degree of the cations. Also, the size of perovskite QDs plays an important role on their optical properties due to quantum confinement effect [16].

3. Chemical synthesis of perovskite QDs

3.1. Synthesis of $MAPbX_3$ QDs

Perez-Prieto and coworkers pioneered the wet chemistry colloidal synthesis of free-standing hybrid perovskite QDs ($MAPbBr_3$ in their case) [17]. A simple one-step approach was employed in their experiment. The $PbBr_2$ was reacted directly with a mixture of ammonium bromide with short methyl chain and longer alkyl chains. In the middle part of the crystal, the MA cations were embedded, which would connect the neighboring $[PbBr_6]^-$ octahedra. And, the outer space will be occupied by the longer alkyl ammonium cations; as a result, the growth of $MAPbBr_3$ nanocrystals (NCs) is terminated. Therefore, one could assume that the longer alkyl ammonium cations in the outer space played the role of capping ligands of the perovskite NCs, which may be the reason that the $MAPbBr_3$ NCs could be dispersible in many solvents. That is to say that the role of these ligands is to provide a self-termination of the crystallization, leading to the formation of discrete nanoparticles in solution. In their case, the resulting $MAPbBr_3$ QDs could be stable for concentrated solutions as well as in solid states for 3 months. The corresponding microstructure of the synthesized products was shown in **Figure 2a**, in which a mixture of nanodots (~10 nm) and nanoplatelets (~40 nm) could be distinguished. **Figure 2b** and **c** shows the absorption and PL spectra of these highly crystalline $MAPbBr_3$ QDs, and a high-purity green emission at about 530 nm can be found. The corresponding PL quantum efficiency was about 20%.

By optimizing the molar ratio of octylammonium bromide:MA bromide:$PbBr_2$ (8:12:5) in a typical reprecipitation method while maintaining the 1-octadecene:$PbBr_2$ molar ratio of 62.6:1.0, this research group promoted the quantum efficiency of $MAPbBr_3$ QDs to 83% [18], demonstrating a promising potential for use in luminescent devices, such as LEDs and laser diodes. Owing to the fact that surface states in QDs would support the desired passivation treatment, Perez-Prieto and colleagues improved the organic capping of the $MAPbBr_3$ QDs; as a result, intensely luminescent and easily dispersible $MAPbBr_3$ QDs were produced, as shown in **Figure 2d**. As for the origin of the surface states, Li et al. recognized that the richness of halogen at the surface of QDs ought to be responsible for surface states [19]. On the one hand, abundant Br atoms at the surface will connect with cations, inhibiting the trapping of excited carriers and then high PL quantum efficiency. This process can be named as self-passivation effect, which is similar to the intentional passivation behaviors of traditional QDs with halogen ions. On the other hand, riched Br on surface should be binded with MA to form $PbBr_x$ analogs, which possesses a relatively large bandgap of 4.0 eV. Therefore, quasi-core-shell structure of $MAPbBr_3$/Br was formed. This superior characterization is similar as the shelling of ZnS around CdSe QDs core, photoexcitated carriers would be confined, and a high PL quantum efficiency could be expected. For a further confirmation, Zhong and

coworkers performed the energy-dispersive spectroscopy measurements for synthesized $MAPbBr_3$ QDs [20]. They found a Br/Pb ratio of 3:5 for QDs with an average diameter of 3.3 nm, matching with the observation in Li's report. Also, the X-ray photoelectron spectroscopy results for $MAPbBr_3$ QDs support their argument above, and the smaller the diameter of QDs, the larger the ratio of Br/Pb.

Subsequently, this simple synthetic method was adopted in other groups, and an increasing number of papers have been published in this field. For example, Luo and coworkers used either octylammonium bromide or octadecylammonium bromide to produce perovskite QDs by using the reprecipitation method, with the size of QDs of 3.9 and 6.5 nm, respectively [21]. In their case, the size control of QDs was due to the different ligand-binding kinetics, and the high solubility of longer hydrophobic chain ligands could facilitate the increase of QD size. Zou et al. developed a ligand-assisted reprecipitation strategy to fabricate highly luminescent and color-tunable colloidal $MAPbBr_3$ QDs with the absolute quantum efficiency up to 70% at room temperature (RT) and low excitation fluencies. In their work, the reprecipitation method was a simple way for preparing organic nanocrystals or polymer dots simultaneously through the solvent mixing [22]. As shown in **Figure 3a**, they employed the same principle and simply mix a solution of $MAPbX_3$ precursors in good solvent (*N*-dimethylformamide (DMF)) into a vigorously stirred poor solvent (toluene, hexane, etc.) to form the organometal halide perovskites. Simultaneously, the long-chain organic ligands, such as n-octylamine and

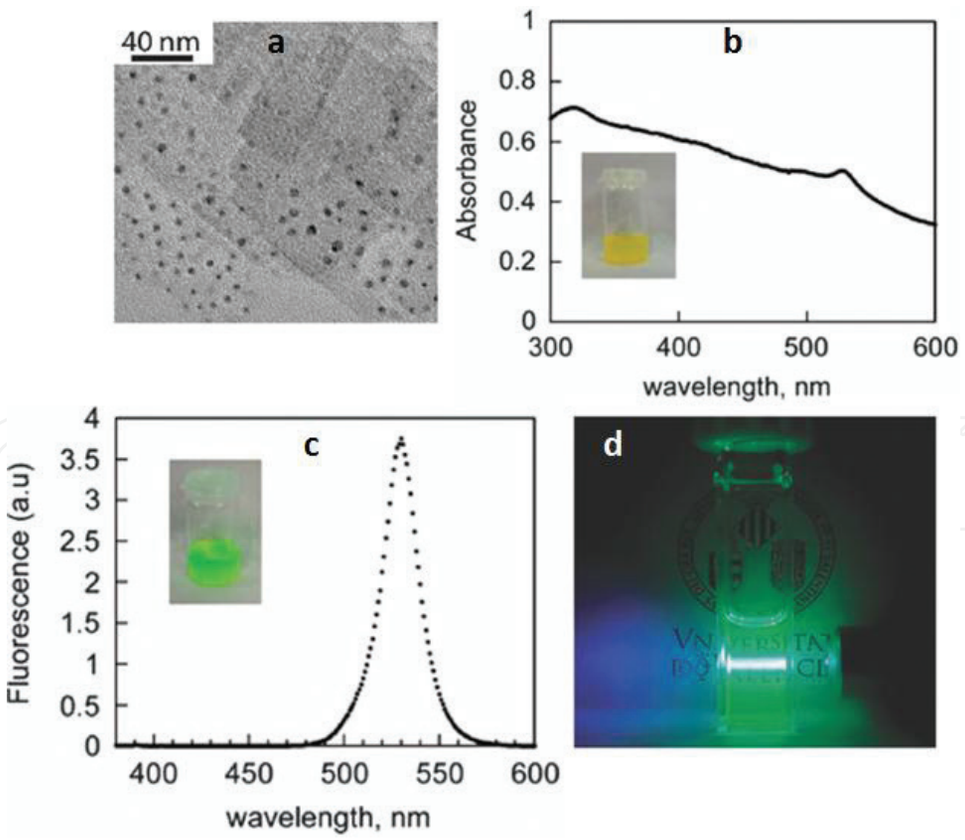

Figure 2. (a) Transmission electron microscope image of $MAPbBr_3$ QDs with a mixture of nanodots and nanoplatelets. (b) UV-visible absorption and (c) PL spectra of the $MAPbBr_3$ QDs. (d) Image of the toluene dispersion of $MAPbBr_3$ QDs under UV-laser pointer excitation.

oleic acid (OA), were introduced into a mixture to control the crystallization of precursors into colloidal QDs. So, it can be assumed that n-octylamine controlled the kinetics of crystallization and further contributed to the size control of $MAPbX_3$ QDs, whereas OA suppressed the aggregation effects and ensures their colloidal stability. **Figure 3b** shows the typical transmission electron microscopy image of $MAPbBr_3$ QDs, which were quasi-spherical and had an average diameter of 3.3 nm with a size deviation of ±0.7 nm. In addition, the simple ligand-assisted reprecipitation approach can be easily extended to fabricate colloidal $MAPbX_3$ QDs through halide substitutions. By mixing of PbX_2 slats in the precursors, a series of QDs with tunable compositions and emission wavelengths were prepared. **Figure 3c** shows the PL spectra and optical images of these samples under sunlight and an UV lamp (365 nm).

3.2. Synthesis of $CsPbX_3$ QDs

Colloidal synthesis routes of all-inorganic $CsPbX_3$ QDs have also been developed, and such novel QD systems have been receiving increasingly significant attention, which is assumably due to the reason that $CsPbX_3$ QDs possess higher stability than that of organic-inorganic hybrid $MAPbX_3$ QDs. Following the traditional hot-injection approach which is commonly used for the synthesis of metal chalcogenide QDs, Kovalenko and coworkers firstly synthesized the monodisperse $CsPbX_3$ QDs with a high degree of compositional bandgap engineering [23]. In their report, the Cs precursors were injected into the lead halide precursors, which contained the hot, high boiling point solvents. OA and oleylamine were mixed to dissolve the lead halide sources and to stabilize the QDs. By using the in situ PL measurements, they observed an interesting phenomenon that the reaction process after the Cs precursor injection was very quick. Within several seconds, the synthesis of the majority of $CsPbX_3$ QDs was realized. For the above synthesis method with a very rapid process, the unit size of $CsPbX_3$ QDs depends strongly on

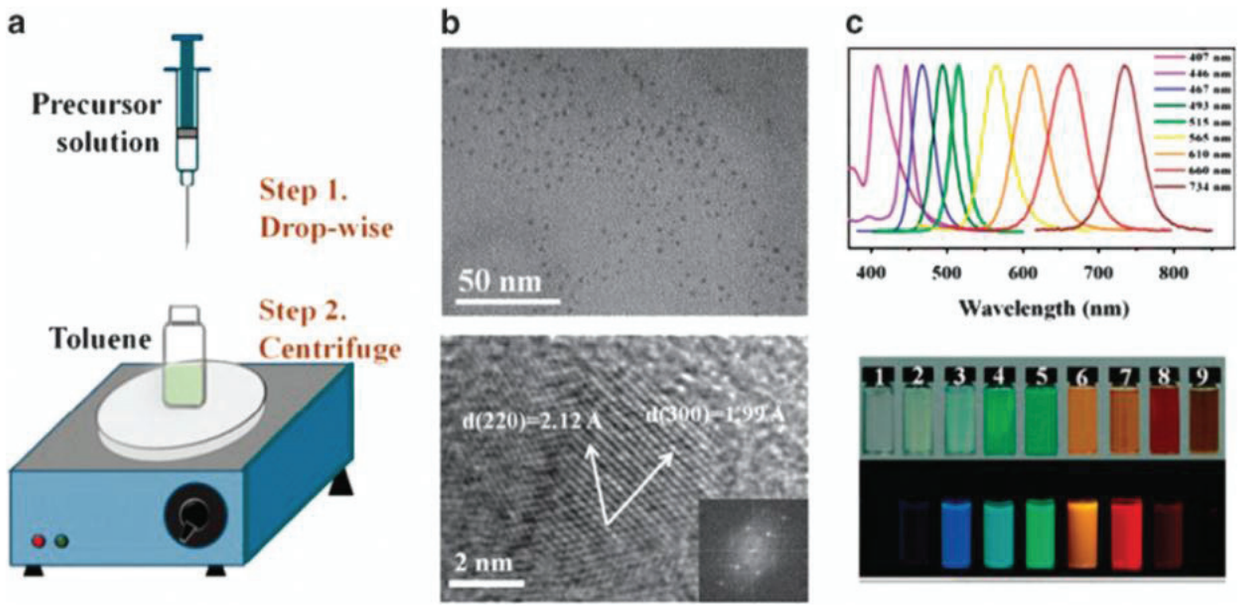

Figure 3. (a) Schematic illustration of the reaction system and process of ligand-assisted reprecipitation method. (b) Transmission electron microscope images of the produced $MAPbBr_3$ QDs. (c) PL emission spectra of the $MAPbX_3$ QDs and the corresponding optical images of colloidal $MAPbBr_3$ QDs solutions under ambient light and a 365 nm UV lamp.

the reaction temperature, and the size of the QDs decreases by decreasing the reaction temperature. In their study, the $CsPbX_3$ QDs were produced with tunable size from 4 to 15 nm. Note that $CsPbX_3$ QDs crystallized in the cubic phase in their case rather than the tetragonal or orthorhombic phases at high temperature, as shown in **Figure 4a** and **b**. More importantly, the emission wavelength or photon energy of the resulting $CsPbX_3$ QDs was tunable over the entire visible spectral region (410–700 nm) by varying the ratios of the precursor salts ($PbCl_2$/$PbBr_2$, $PbBr_2$/PbI_2). As shown in **Figure 4c** and **d**, the obtained $CsPbX_3$ QDs exhibit continuously tunable PL emission with a narrow linewidth of 12–42 nm and also a superior PL quantum yield up to 90%. Such an excellent optical performance is interesting, considering the facile synthesis route which involves neither core-shell structure nor surface modifications. Later on, by means of a droplet-based microfluidic platform, allowing for online absorption/PL measurements, the same research group investigated the formation mechanisms of such perovskite QDs.

In addition to the hot-injection technique, RT reprecipitation methods have also been proposed and developed for the controllable synthesis of $CsPbX_3$ QD system. For instance, Huang et al. reported the emulsion-based synthesis of perovskite nanocrystals involving many morphologies at RT [20]. Li et al. reported that the $CsPbX_3$ QDs can be synthesized at RT, which was similar to the ligand-assisted reprecipitation method used for $MAPbX_3$ QD system [19].

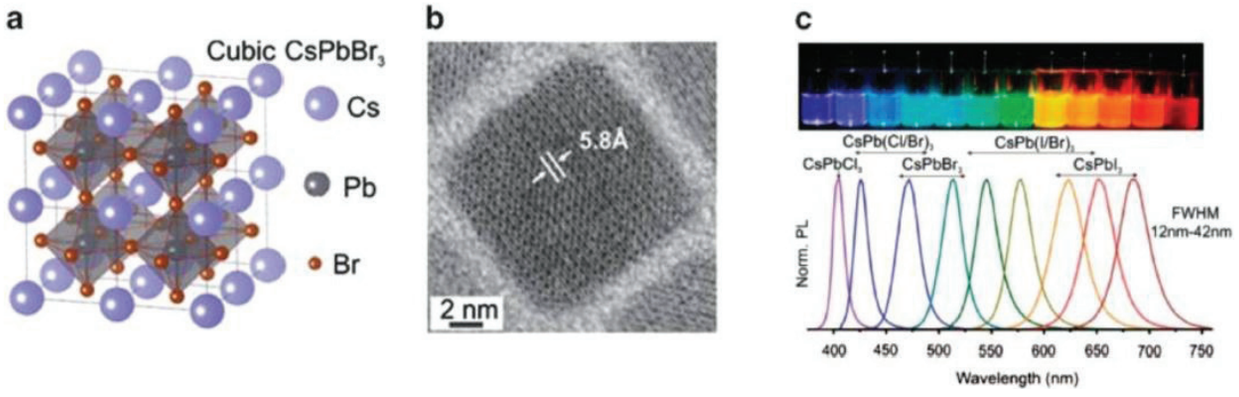

Figure 4. Monodisperse $CsPbX_3$ QDs and their structural characterization. (a) Schematic of the cubic perovskite lattice and (b) typical microstructure image of $CsPbX_3$ QDs. (c) Colloidal $CsPbX_3$ QDs exhibiting composition-tunable bandgap energies covering the entire visible region with narrow and bright emission (colloidal solutions in toluene under UV lamp).

4. Synthesis of perovskite QDs through halide ion exchange reaction

4.1. Synthesis of $MAPbX_3$ QDs

A post-preparative halide ion exchange on perovskite QDs provides an additional means to modify their composition and thus the optical characterizations while preserving their size and morphology. Jang et al. reported the reversible halide exchange reaction of organometal trihalide perovskite colloidal QDs for full-range bandgap tuning [24]. **Figure 5a** shows a schematic of the reversible halide exchange reaction of $MAPbX_3$ QDs with MAX, where X = Cl, Br, and I. The $MAPbX_3$ can be converted to any composition ones using MAX in isopropyl solution at RT. In their case, the synthesis of composition-tuned $MAPbBr_{3-x}Cl_x$ and $MAPbBr_{3-x}I_x$ was carried out by

the Br exchange reaction of $MAPbBr_3$. As the starting material, $MAPbBr_3$ QDs were synthesized using a mixture of 1:1 MABr:$PbBr_2$ dissolved in octylamine and (octadecene) ODE. Octylamine serves as the capping ligands for the QDs. Then, $MAPbBr_3$ QDs were added into a MACl- or MAI-dissolved isopropyl solution affording $MAPbBr_{3-x}Cl_x$ and $MAPbBr_{3-x}I_x$, respectively. As shown in **Figure 5b**, the composition of the mixed halide perovskite QDs can be easily distinguished by their colors. **Figure 5c** shows the UV-visible diffuse reflectance spectrum of all produced samples (10 μm thick films on silicon substrates). The composition tuning of these samples enabled the bandgap to display absorption over a wide range of 400–850 nm, corresponding to the photon energy of 1.5–3.1 eV. The corresponding PL spectra of these samples were also measured and put together on a normalized scale for a comparison. Note that the emission intensity of $MAPbBr_{3-x}Cl_x$ and $MAPbBr_{3-x}I_x$ significantly decreases with increasing x, matching with other reports either for perovskite QDs or films. The anion-exchange method is also possible in the solid phase, as demonstrated by Yang and coworkers [25]. Following a solution-phase growth of $MAPbBr_3$ nanorod arrays, they were subsequently converted to $MAPbI_3$ with similar morphology via a low-temperature annealing at ~140°C in MAI vapor. Such an approach was further confirmed to be feasible by constructing heterostructured LEDs, with $MAPbBr_3$ nanorods exhibiting a green EL emission at 533 nm and $MAPbI_3$ nanorods emitting a red emission at 782 nm.

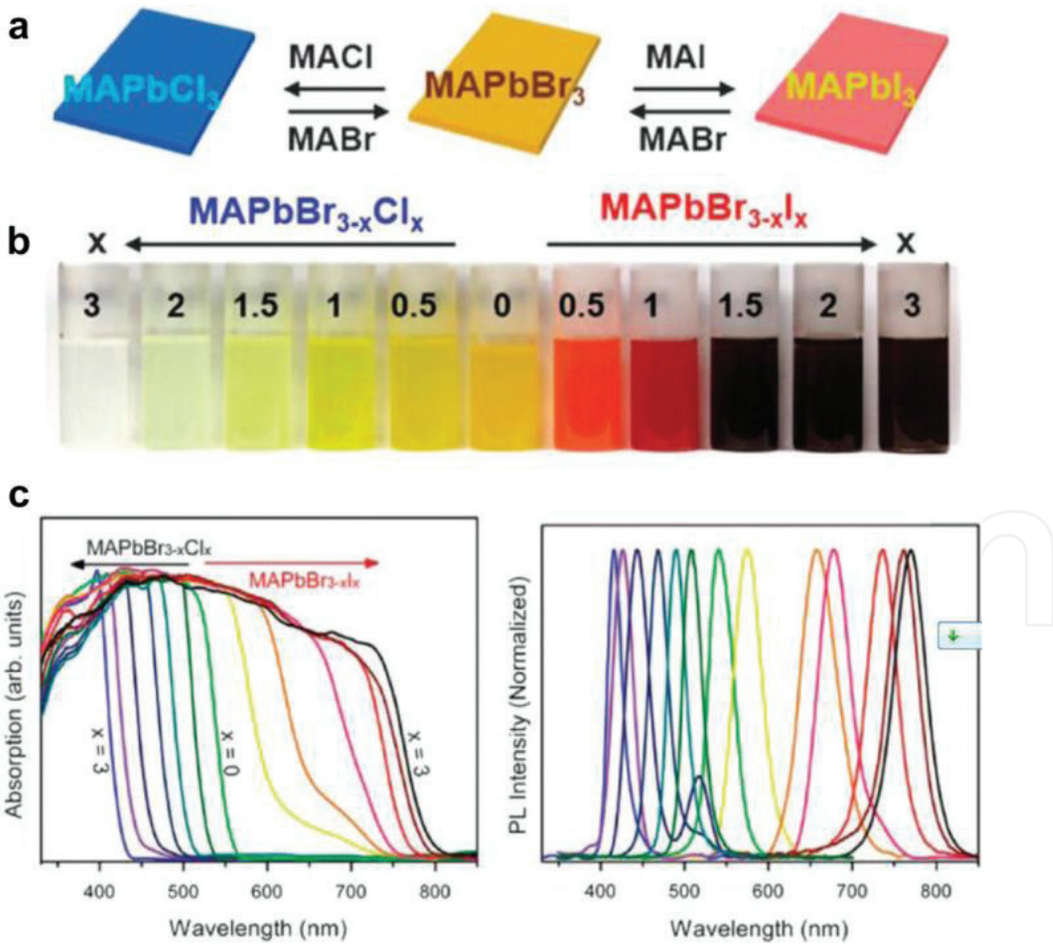

Figure 5. (a) Schematic of anion-exchange reactions for $MAPbX_3$ QD synthesis. (b) Photographs of mixed-halide $MAPbBr_{3-x}Cl_x$ and $MAPbBr_{3-x}I_x$ QDs under room light. (c) UV-visible absorption and RT PL spectra of $MAPbBr_{3-x}Cl_x$ and $MAPbBr_{3-x}I_x$ QDs.

4.2. Synthesis of $CsPbX_3$ QDs

As for the synthesis of $CsPbX_3$ QDs by halide ion exchange, Kovalenko and coworkers and Manna and coworkers have almost simultaneously reported this method for $CsPbX_3$ (X = Cl, Br, I) QD systems [26, 27], tuning their emission wavelength over the spectra range of 410–700 nm, as shown in **Figure 6a** and **b**. In their cases, five kinds of halide ion sources were investigated for ion exchange reaction, oleyammonium/octadecylammonium/tetrabutylammonium halides, organometallic Grignard reagents, and PbX_2 salts. An interesting observation was that the anion-exchange reaction between different halide ions is very fast, and the halide ions could achieve exchange reaction within seconds. A blueshift trend includes I^- to Br^- and Br^- to Cl^- routes, and, similarly, a redshift trend includes Cl^- to Br^- and Br^- to I^- routes, respectively. An important fact should be pointed out that a little size variation for $CsPbX_3$ QDs can be distinguished after the anion-exchange reaction, but the shape of the produced QDs was identical to their original appearance (parent QDs). Also, there was no change on the crystal structure of the produced QDs. Additionally, the ion exchange reaction process did not induce the undesired formation of any remarkable lattice and/or surface defects. As a result, the optical properties of anion-exchanged $CsPbX_3$ QDs are remarkable, including the linewidth and PL quantum yield, and comparable with those directly synthesized through the hot-injection method introduced above.

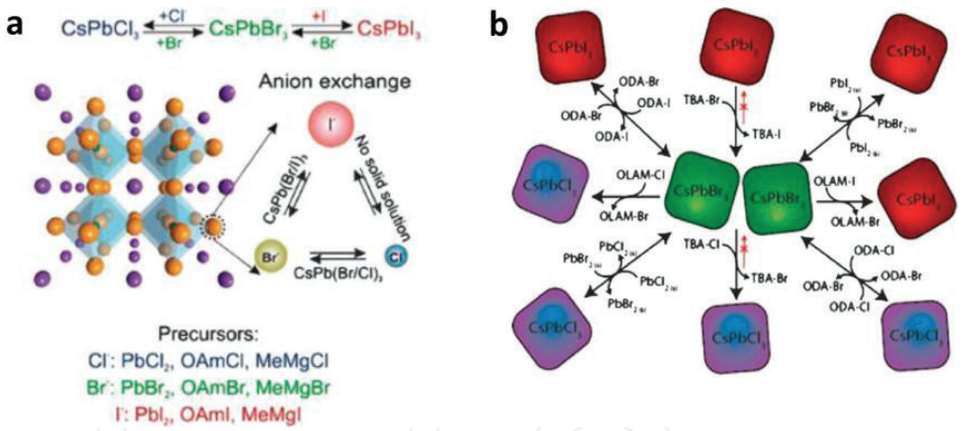

Figure 6. (a) Schematic representation of possible anion-exchange reactions within the crystal structure of $CsPbX_3$ crystal lattice, with indication of suitable reagents. (b) Different routes and precursors for $CsPbX_3$ (X = Cl, Br, I) ion exchange.

5. Optical properties of perovskite QDs

5.1. Exciton-related emission of perovskite QDs

Perovskite QDs exhibit remarkable optical properties, such as the high emission purity, large quantum yield, as well as tunable emission wavelength by varying the constituent elements, size, or dimensions. In the initial stage, most of the researches focused on the synthesis of the perovskite QDs and also their integration into device applications. But, it would be more interesting in our opinion if the optical properties of perovskite QDs or films made out of perovskite QDs could be investigated in detail. Despite the reported advances

on perovskite-based optoelectronics, a deeper understanding of perovskites photophysical properties must be achieved if these materials are to make a technological impact. For example, as a key parameter controlling the recombination dynamics of photogenerated charges, the localization of exciton or free carrier needs to be specified. It means that the identification of dominant recombination mechanisms in perovskites will help interpret the seemingly counterintuitive facts that perovskites can act as both extraordinary photovoltaic materials and superior optical gain mediums for LED and lasers. In general, photovoltaic materials require efficient separation of photocarriers, and emissive materials require high recombination rates [28]. If the obtained exciton-binding energy of the perovskites is comparable to the thermal energy at RT (~26 meV), excited states will tend to dissociate into free carriers rather than recombination radiatively. The photoexcitation of perovskites can lead to the formation of free carriers and excitons, which then recombine to emit photons corresponding to the bandgap of perovskites. Although the question over the dominant species is still under investigation, it is generally accepted that free carriers are prevalent in perovskite films. Even et al. claimed that free carriers are photoexcited at RT, where Wannier-Mott excitons are dominant at low temperatures [29]. As for perovskite QDs, several groups have used temperature-dependent PL measurements to study the competition between exciton and free carriers. In Shi's study, temperature-dependent PL measurements were carried out to understand the optical transition mechanisms of the $CsPbBr_3$ QDs [30]. As shown in **Figure 7a**, with the decrease of the temperature, only one emission peak can be solved, indicating the absence of structural phase transition. And, the strong excitonic emission behavior was verified by performing the power-dependent PL measurements. As shown in **Figure 7b**, a power law dependence with $\beta = 1.31$ confirms the excitonic characteristics of the spontaneous emission. Moreover, by plotting the emission intensity of $CsPbBr_3$ QDs *versus* temperature, thermally activated nonradiative recombination process was observed, as shown in **Figure 7c**. Exciton-binding energy of the $CsPbBr_3$ QDs was further achieved by the following equation:

$$I(T) = \frac{I_0}{1 + A\exp\left(-\frac{E_B}{KT}\right)} \quad (1)$$

where K is the Boltzmann constant, T is the temperature, I_0 is the emission intensity at 0 K and A is a proportional constant. From the fitting, a value of 43.7 ± 4.9 meV for E_B was extracted. The data are much higher than the thermal energy at RT and ensure exciton survival well above RT. Therefore, they argued that the observed PL performance originates from the exciton-related emission. However, many studies attributed the PL spectra at RT to free carrier recombination. For example, D'Innocenzo et al. stated that excitons generated by low-density excitation were almost fully ionized at RT when the exciton-binding energy is moderately larger than the thermal energy at RT [31]. As shown in **Figure 7d**, the exciton-phonon interaction in carrier recombination process for $CsPbBr_3$ QDs was also investigated in Shi's report by studying the linewidth broadening behavior of $CsPbBr_3$ QDs. The value of optical phonon energy of 36.3 ± 1.8 meV was derived.

5.2. Quantum confinement effect in perovskite QDs

As we mentioned above, the optical properties of perovskite QDs depend not only on the constituent halide ions but also on their size or diameter. As we all know, quantum confinement effect has been widely studied in conventional semiconductor nanomaterials. Also, the

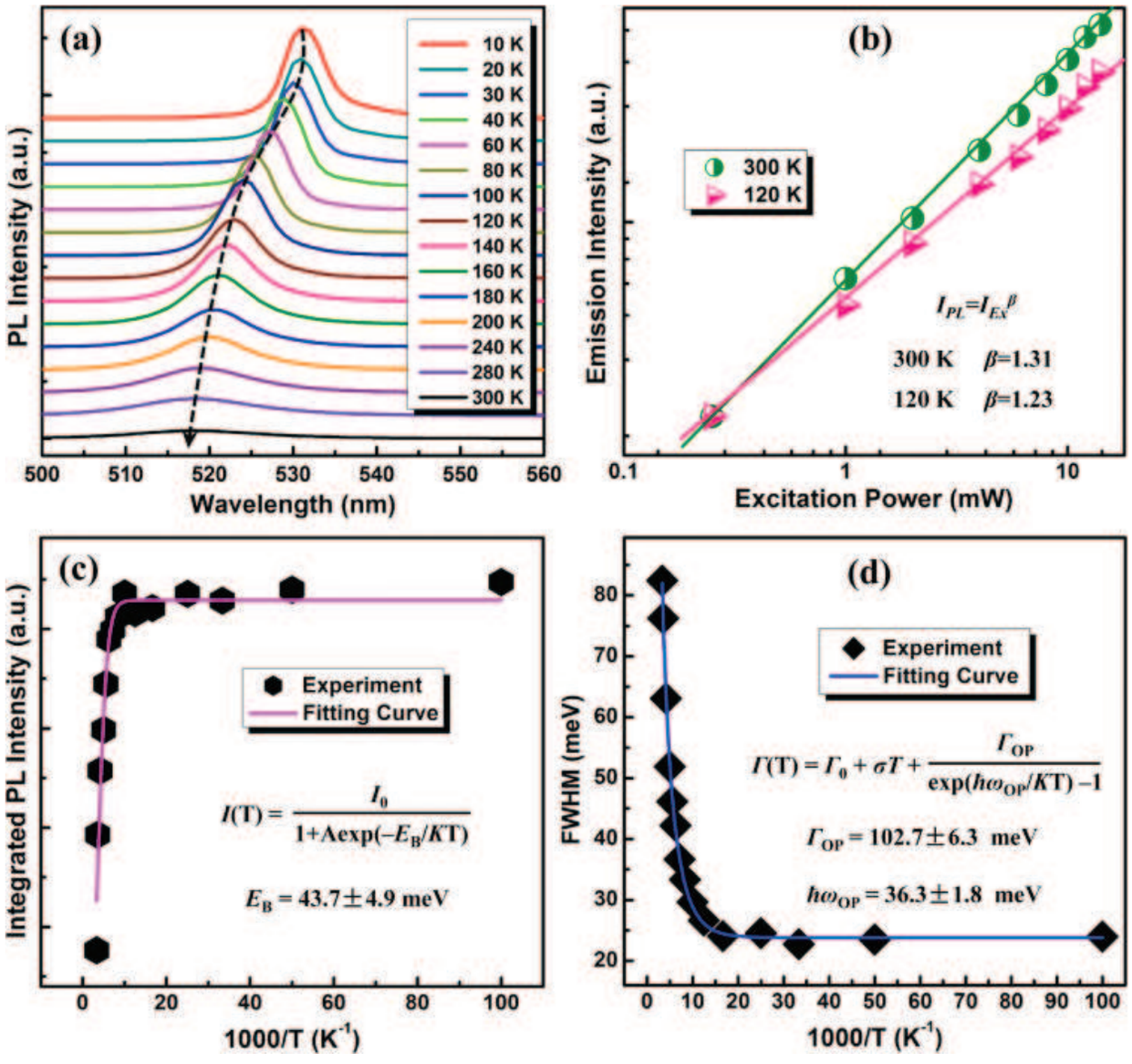

Figure 7. (a) Temperature-dependent PL spectra of the $CsPbBr_3$ QDs taken from 10 to 300 K. (b) The relationship between the integrated PL intensity and the excitation power of the $CsPbBr_3$ QDs at 300 and 120 K. (c) Integrated PL intensity and (d) linewidth of the $CsPbBr_3$ QDs as a function of reciprocal temperature from 10 to 300 K.

latest development in the size-controlled synthesis of perovskite QDs has enabled detailed investigations of quantum confinement effect in QDs. Friend and coworkers observed size-dependent photon emission from $MAPbBr_3$ QDs embedded in an organic matrix [16], where the QD size and their PL peak could be tuned by varying the concentration of the precursors. In their case, a $MAPbBr_3$ precursor solution (MABr and $PbBr_2$ dissolved in *N*,*N*-dimethylformamide) and 4,4-bis(*N*-carbazolyl)-1,1-biphenyl (CBP) matrix solution were prepared and mixed to achieve various weight ratios between CBP and the perovskite precursor. They firstly determined the average size of perovskite QDs by using X-ray diffraction, as shown in **Figure 8a**. As the concentration of perovskite QDs decreased, a reduced peak intensity accompanied by peak broadening was observed for (1 0 0) and (2 0 0) diffraction peaks, indicating a reduction of the size of nanocrystallites. Accordingly, the PL peak gradually shifted to higher energy decreasing the particle size, as shown in **Figure 8b**. They also summarized the changing trend by fitting with the equation of $E_{PL} = 2.39 + 12/d^2$ eV (**Figure 8c**),

in which *d* is the particle size in nanometer. This suggested that the PL blueshift is a manifestation of quantum confinement of excitons in the perovskite nanocrystals. **Figure 8d** shows the corresponding absorbance data of the produced $MAPbBr_3$ QDs with different sizes, and a monotonic shift of the absorption edge toward the higher energies matched the above observation in PL spectra.

Quantum confinement effects have also been observed in all-inorganic $CsPbBr_3$ QDs. Kovalenko and coworkers reported the size-dependent PL emission from square-shaped $CsPbBr_3$ QDs [23], in which the PL emission peak gradually blueshifted from 512 to 460 nm as the diameter of QDs decreased from 11.8 to 3.8 nm, as shown in **Figure 9a**. **Figure 9b** shows the experimental and theoretical size dependence of the bandgap of $CsPbBr_3$ QDs in their case. In addition, tunable PL from $CsPbBr_3$ nanocrystals by varying the number of layers has also been reported, and the corresponding bandgap energy increases with the decreasing the number of layers. Alivisatos and coworkers reported the synthesis of quantum-confined highly fluorescent $CsPbBr_3$ nanoplatelets [32]. Their observations show that the thickness of $CsPbBr_3$ nanoplatelets can be tuned from 1 to 5 unit cells by changing the reaction temperature, with the monolayer platelets emitting at 400 nm, whereas the bulk-like crystals emitted at 520 nm.

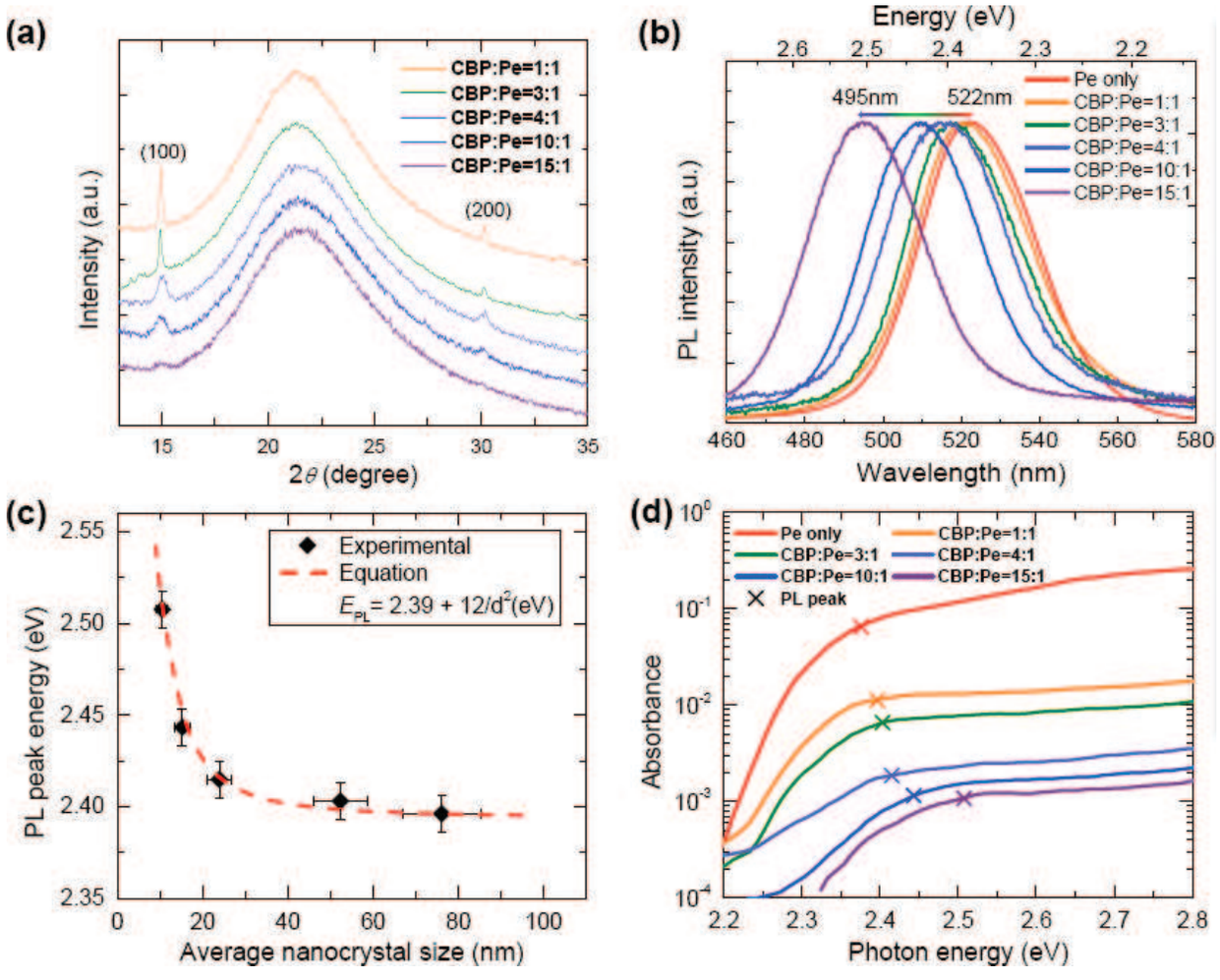

Figure 8. (a) X-ray diffraction patterns and (b) PL spectra of CBP:$MAPbBr_3$ with various weight ratios. (c) Energy of PL emission peak as a function of average perovskite nanocrystal size. (d) Absorbance data of the produced samples.

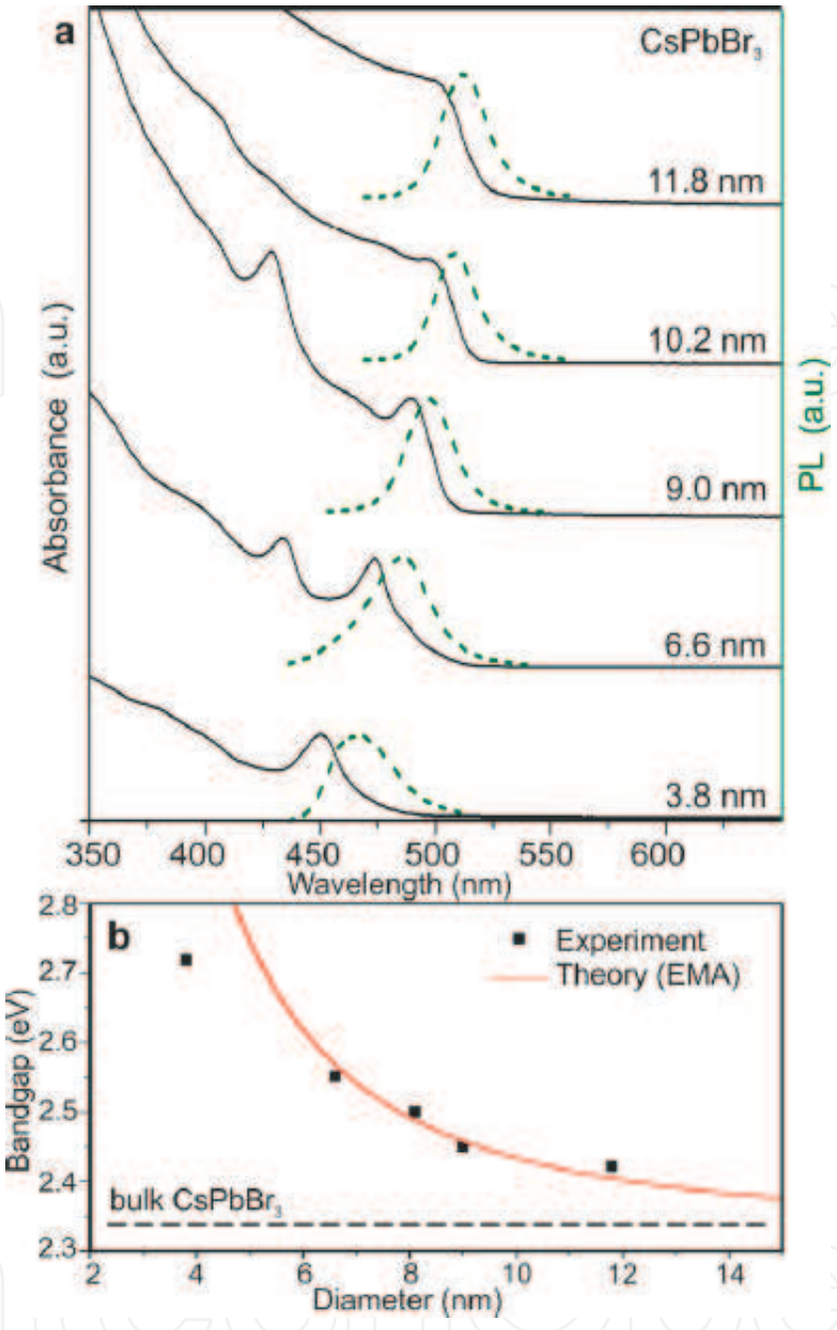

Figure 9. (a) Quantum size effects in the absorption and emission spectra of 5–12 nm $CsPbBr_3$ QDs. (b) Experimental *versus* theoretical (effective mass approximation (EMA)) size dependence of the bandgap energy.

6. Perovskite QD LEDs

6.1. Structure of perovskite QDs LEDs

As we mentioned above, perovskite QDs have been shown to possess high PL quantum yield, high emission purity, and tunable emission wavelength that make them suitable for high-performance, low-cost, and lightweight LEDs. Perovskite materials were incorporated into

LEDs functioning at liquid nitrogen temperature back in the 1990s, and RT-working bright LEDs were fabricated by solution processing of hybrid perovskites by Tan et al. [33]. In their device, a solution-processed $MAPbI_{3-x}Cl_x$ perovskite layer was sandwiched between TiO_2 and poly(9,9-dioctylfluorene) (F8) layers for effective radiative recombination of electrons and holes in the perovskite layer. Also, using $MAPbBr_3$-emissive layer, an architecture of ITO/PEDOT:PSS/$MAPbBr_3$/F8/Ca/Ag was fabricated, producing a luminance of 364 cd/m^2 at a current density of 123 mA/cm^2. Because of the significantly higher quantum efficiency of perovskite QDs than that of perovskite bulk films, superior device performance for perovskite QD LEDs could be expected [34]. A typical perovskite QD LED consists of an intrinsic active layer in a double-heterojunction structure. As shown in **Figure 10**, an n-type electron transport layer and a p-type hole transport layer are usually used to construct a typical perovskite QD LED. Under forward bias, the injection of charge carriers into a thin luminescent layer leads to radiative recombination and provides light emission in all directions. Efficient LEDs use electrodes that readily inject carriers into the active region and prevent charges from passing through the device and quenching at contacts. Since the work of Tan et al. in 2014 [33], various perovskite QD LEDs using different perovskite active layers and electron/hole transport layers have been reported.

6.2. LEDs based on perovskite QDs

Song and coworkers firstly reported the perovskite QD LEDs with tunable emission wavelength based on $CsPbBr_3$ QDs [4]. For the device structure of ITO/PEDOT:PSS/PVK/QDs/TPBi/LiF/Al (shown in **Figure 11a**), the luminescence of blue, green, and orange LEDs reached 742, 946, and 528 cd/m^2, with external quantum efficiency of 0.07, 0.12, and 0.09%, respectively. In addition, the produced LEDs possess narrow linewidths, indicating their potential applications in displays. However, non-optimized devices exhibited poor emission efficiency. Generally, in order to improve the device performance, three important factors should be considered: carrier

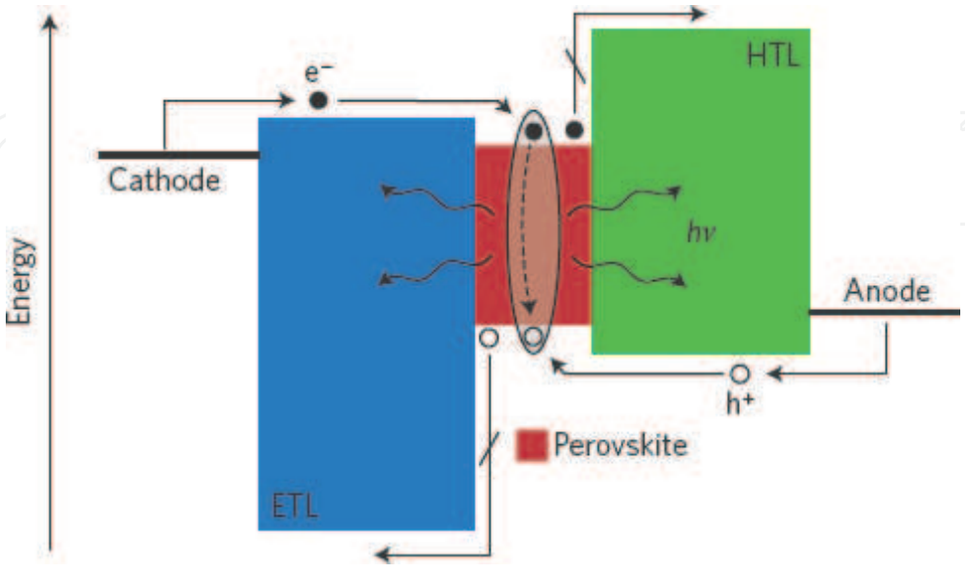

Figure 10. General device structure of perovskite QD LEDs. ETL, electron transport layer; HTL, hole transport layer.

injection efficiency, radiative recombination efficiency, and injection balance. For an improved carrier injection efficiency, a thin perfluorinated ionomer film was introduced between the hole transport layer and $CsPbBr_3$ QDs active layer in Zhang's study [35]. In their case, the hole injection efficiency was enhanced greatly, which favored a high brightness. Besides, the usage of carrier transport layers with a high conductivity could ensure a high carrier injection efficiency, resulting in an improved external quantum efficiency.

In order to promote the carrier radiative recombination efficiency, the undesired lattice and surface/interface defects should be excluded. Sun's research group found an interesting phenomenon that the introduction of $CsPb_2Br_5$ QDs attached on $CsPbBr_3$ QDs could improve the emission lifetime by decreasing nonradiative energy transfer to the trap states via controlling the trap density [36]. As a result, a high external quantum efficiency of about 2.21% was achieved, and a maximum luminance of 3853 cd/m^2 was obtained. **Figure 12a** shows the X-ray diffraction patterns of the synthesized perovskite QD products. The peak located at 30.36° is assigned to (2 0 2) diffraction of $CsPbBr_3$, whereas the peak at 30.69° is identified from $CsPb_2Br_5$. And, the impurities of $CsPb_2Br_5$ phase were emerged in the low-temperature (70°C) solution-processed $CsPbBr_3$ products. The generation of the secondary phase $CsPb_2Br_5$ in the product can be ascribed to the following process: $PbBr_2 + CsPbBr_3 \rightarrow CsPb_2Br_5$. **Figure 12b** displays the schematic diagrams of the corresponding crystal structures of the $CsPbBr_3$ and $CsPb_2Br_5$ QDs. They further fabricated the LED device by constructing the heterostructure shown in

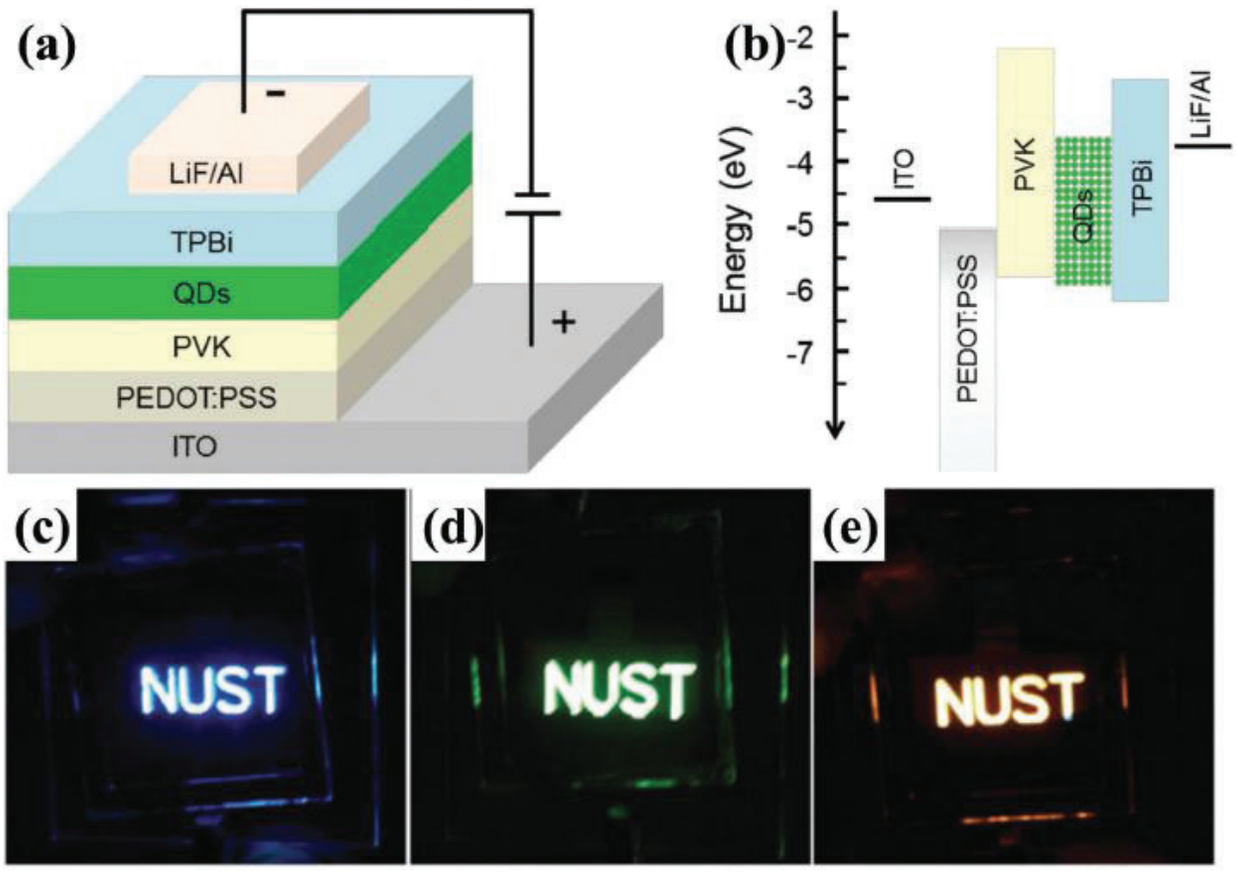

Figure 11. (a) Structure of the perovskite LED device. (b) Energy band alignment of the device. (c–e) Blue, green, and orange LEDs with abbreviations of NUST.

Figure 12c and achieved a high-purity green emission at about 527 nm. The inset of **Figure 12d** shows the corresponding photograph of a device with an active area of 2 × 2 mm^2. In fact, contradiction exists about carrier radiative recombination efficiency and injection efficiency. For example, to keep a high quantum yield, surface passivation is usually necessary, while long-chain ligands will reduce the conductivity of QDs. In this regard, Pan and coworkers applied a short ligand, di-dodecyl dimethyl ammonium bromide, to passivate $CsPbBr_3$ QDs and facilitate the carrier transport ability [37]. Consequently, a promoted PL quantum yield of about 71% was achieved, and a higher external quantum efficiency of ~3.0% was obtained.

As discussed above, the carrier injection efficiency, radiative recombination efficiency, and injection balance are important factors for the device performances of perovskite QD LEDs. In fact, the QDs applied in previous reports were not well purified due to the continuous growth with classical purification strategies. Recently, Zeng's group developed a handy surface purification method that can achieve recyclable treatment on QDs using hexane-/ethyl acetate-mixed solvent [38]. Thus, a balance of carrier injection efficiency and surface passivation effect can be constructed, as illustrated in **Figure 13a**. After two purifications, the QDs

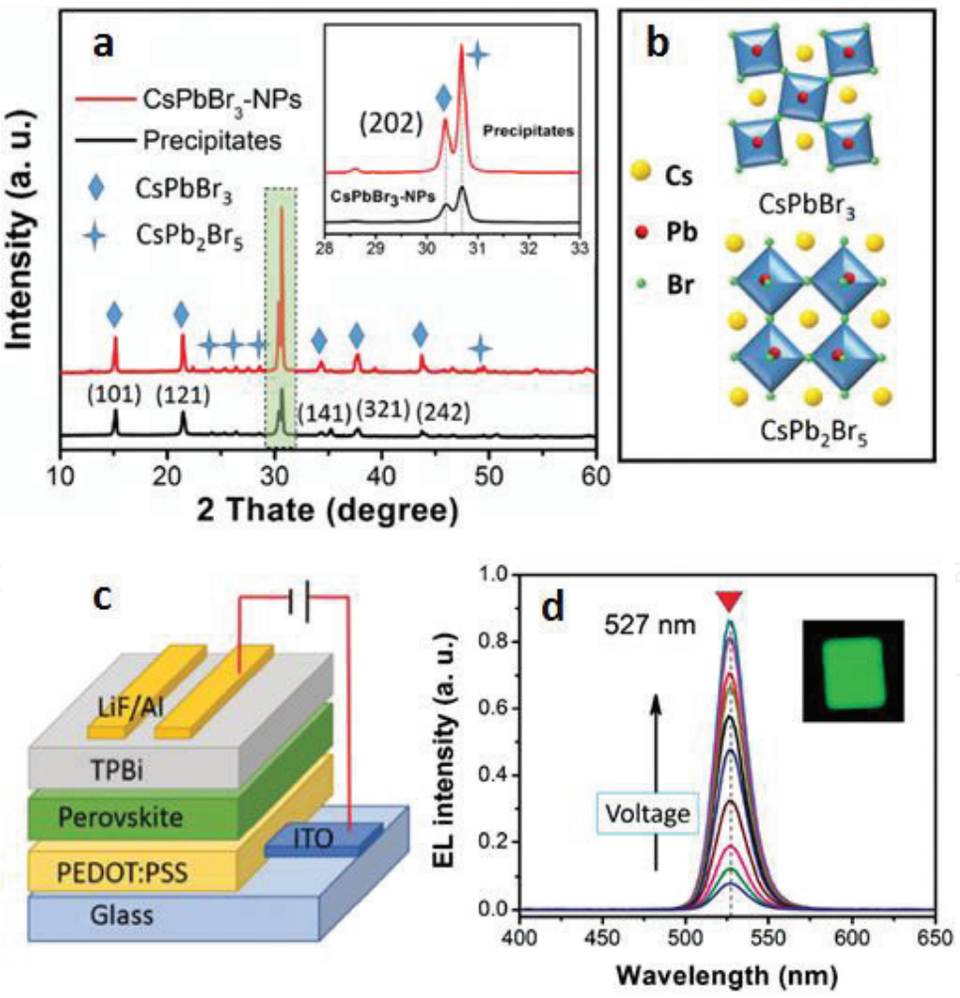

Figure 12. (a) X-ray diffraction patterns of $CsPbBr_3$ QDs and precipitates of products. (b) The schematic diagrams of the corresponding crystal structures of the $CsPbBr_3$ and $CsPb_2Br_5$ QDs. (c) Device structure of the studied perovskite LEDs. (d) EL spectra at different driving voltages. The inset shows the photograph of a device with an active area of 2 × 2 mm^2.

obtained still possess a good stability (shown in **Figure 13b**). But, the PL quantum yield shows no obvious decrease (**Figure 13c**), indicating a good surface passivation. Therefore, we could expect that good dispersivity ensures an excellent film formation ability and pure surface that leads to efficient carrier transport. So, the efficiency of carrier injection was greatly enhanced (shown in **Figure 13d**). In virtue of the above advantages discussed, the luminance (**Figure 13e**) and current efficiency (**Figure 13f**) of the resulting LEDs based on $CsPbBr_3$ QDs are greatly improved compared to previous studies, and more importantly, the studied LED achieves a record external quantum efficiency of 6.27% (**Figure 13g**).

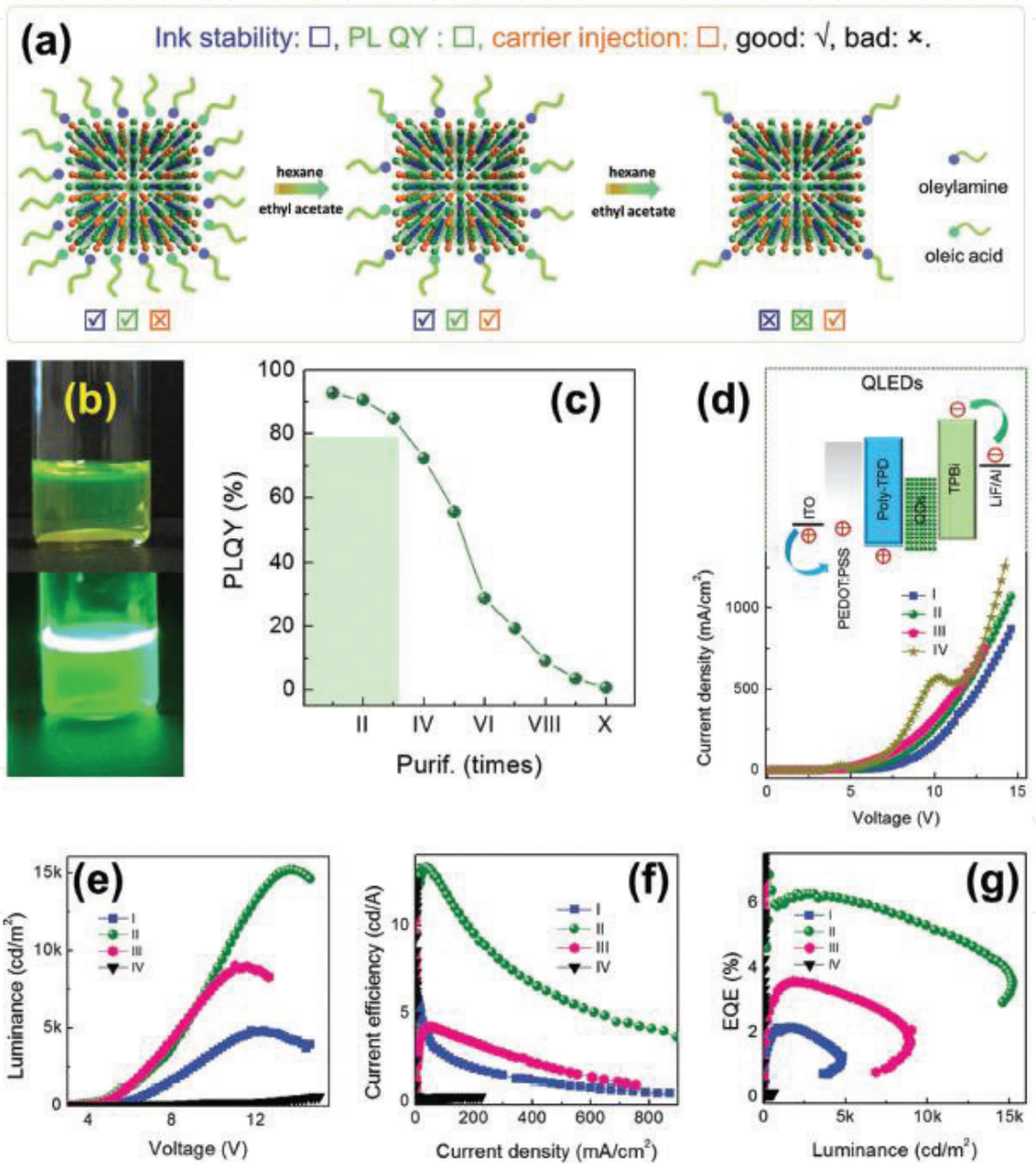

Figure 13. (a) Schematic illustration of the control of ligand density of $CsPbBr_3$ QD surfaces. (b) Photographs of $CsPbBr_3$ QD inks without (upper) and with (below) UV light excitation after two cycles of treatments. (c) PL quantum yield of $CsPbBr_3$ QDs with different purifying cycles. (d) Current density-voltage, (e) luminance-voltage, (f) current efficiency-current density, and (g) external quantum efficiency-luminance characteristics of the perovskite QD LEDs.

http://dx.doi.org/10.5772/intechopen.68275

Although the device performance of perovskite QD LEDs was promoted greatly in a short time, operation stability has always been criticized for such devices in a continuous current mode, which are the main obstacles hindering the reliable device operation and their future application. In previous reports, conventional carrier injection conducting polymer or small molecules, such as PEDOT:PSS, PCBM, and 1,3,5-tris(2-*N*-phenylbenzimidazolyl) benzene, have been frequently employed as the carrier injectors in perovskite LEDs [25, 33, 35, 36], but their inherent chemical instability inevitably degrades the device performance; thus, a high-efficiency light emission cannot be sustained over a long running time. More recently, Shi et al. present a strategy that addresses simultaneously the emission efficiency and stability issues facing current perovskite LEDs' compromise [30]. Wide bandgap semiconductors, n-MgZnO and p-MgNiO, were employed as the electron and hole injectors to construct $CsPbBr_3$ QD LEDs. The resulting diode demonstrates a high luminance (3809 cd/m^2) and external quantum efficiency (2.39%), as well as a significantly improved stability compared with reference and other previously reported devices constructed with organic carrier injectors. **Figure 14a** illustrates the emission intensity of the diode *versus* running time, and one can see that the EL intensity has almost not changed over 30 min. A long-term operation stability measurement demonstrated that the device could operate continuously for 10 h with an emission decay of below 20%, greatly superior to other previously reported devices constructed with organic electron and/or hole transport layers. It is believed that the device concept proposed in their study will provide valuable information for the future design and development of high-efficiency and air-stable perovskite QD LEDs.

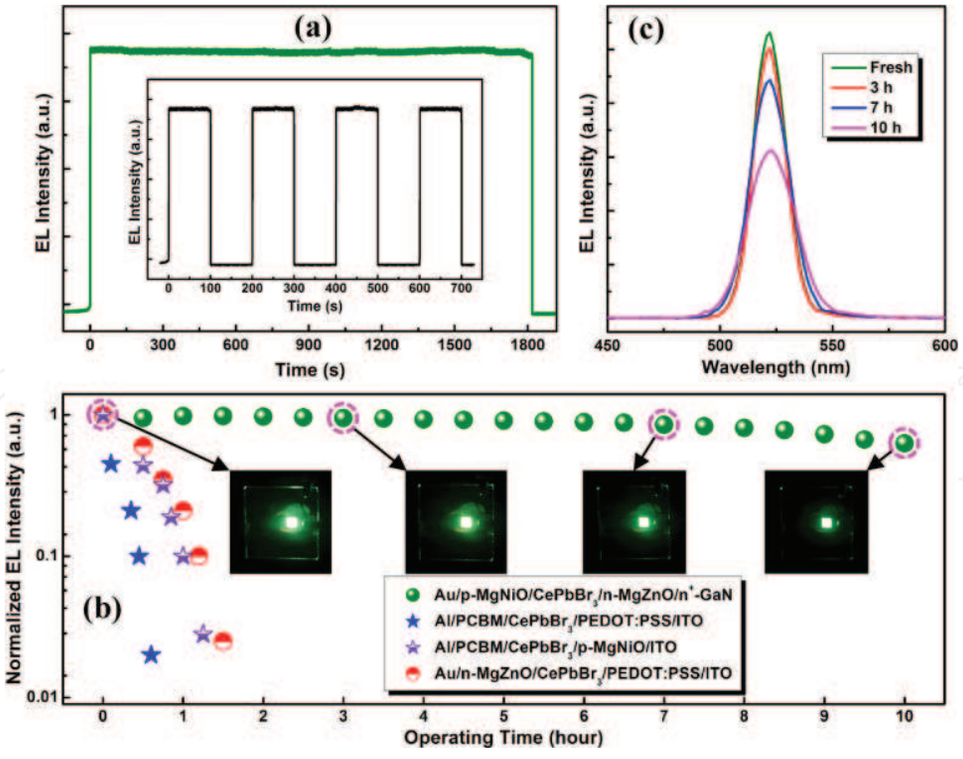

Figure 14. (a) Time dependence (30 min) of the emission intensity of the prepared LEDs at 8.0 V. (b) Emission intensity of the studied LEDs and three reference LEDs as a function of running time under a bias of 10.0 V. The insets show the corresponding photographs of the LEDs after different running periods. (c) Evolution of the emission spectra of the prepared LEDs after different running periods.

7. Summary

In summary, recent developments in perovskite QDs add a new class of members to the family of colloidal QDs. In spite of a short development of only 2 years, perovskite QDs have shown great potential in application in cost-effective LED fields. However, compared with traditional metal chalcogenide QDs, novel synthesis approaches are needed to tailor the surface ligands and enhance the stability of perovskite QDs. At present, the perovskite LEDs based on both organic-inorganic hybrid and inorganic QDs show relatively poor performances, and, therefore, new device structures are required to make a step change in the emission efficiency and operation stability of LEDs. Despite these challenges, we believe that the newly emerging perovskite QDs have a bright future, and the previous studies will provide valuable information for the future design and development of high-performance perovskite QD LEDs.

Author details

Zhifeng Shi*, Xinjian Li and Chongxin Shan

*Address all correspondence to: shizf@zzu.edu.cn

Department of Physics and Engineering, Zhengzhou University, Zhengzhou, China

References

[1] Coe S, Woo WK, Bawendi M, Bulovic V. Electroluminescence from single monolayers of nanocrystals in molecular organic device. Nature. 2002;**420**:800-803

[2] Colvin VL, Schlamp MC, Alivsistors AP. Light-emitting diodes made from cadmium selenide nanocrystals and a semiconducting polymer. Nature. 1994;**370**:354-357

[3] Shirasaki Y, Supran GJ, Bawendi MG, Bulovic V. Emergence of colloidal quantum-dot light-emitting technologies. Nature Photonics. 2013;**7**:13-23

[4] Song J, Li J, Li X, Xu L, Dong Y, Zeng H. Quantum dot light-emitting diodes based on inorganic perovskite cesium lead halides ($CsPbX_3$). Advanced Materials. 2015;**27**: 7162-7167

[5] Qian L, Zheng Y, Xue J, Holloway PH. Stable and efficient quantum-dot light-emitting diodes based on solution-processed multilayer structures. Nature Photonics. 2011;**5**:543-548

[6] Lee KH, Lee JH, Song WS, Ko H, Lee C, Lee JH, Yang H. High efficiency, color-pure, color-stable blue quantum dot light-emitting devices. ACS Nano. 2013;**7**:7295-7302

[7] Shen H, Cao W, Shewnon NT, Yang CC, Li LS, Xue JG. High-efficiency, low turn-on voltage blue-violet quantum-dot-based light-emitting diodes. Nano Letters. 2015;**15**:1211-1216

[8] Jin SY, Lian TQ. Electron transfer dynamics from single CdSe/ZnS quantum dots to TiO_2 nanoparticle. Nano Letters. 2009;**9**:2448-2454

[9] Vybornyi O, Yakunin S, Kovalenko MV. Polar-solvent-free colloidal synthesis of highly luminescent alkylammonium lead halide perovskite nanocrystals. Nanoscale. 2016;**8**: 6278-6283

[10] Buim A, Comin R, Ip AH, Sargent EH. Perovskite quantum dots modeled using ab initio and replica exchange molecular dynamics. Journal of Physical Chemistry C. 2015;**119**: 13965-13971

[11] Tyagi P, Arveson SM, Tisdale WA. Colloidal organohalide perovskite nanoplatelets exhibiting quantum confinement. Journal of Physical Chemistry Letters. 2015;**6**:1911-1916

[12] Wang Y, Li XM, Zhao X, Xiao L, Zeng H, Sun H. Nonlinear absorption and low-threshold multiphoton pumped stimulated emission from all-inorganic perovskite nanocrystals. Nano Letters. 2016;**16**:448-453

[13] Huo C, Cai B, Yuan Z, Ma BW, Zeng HB. Two-dimensional metal halide perovskites: Theory, synthesis, and optoelectronics. Small Methods. 2017;1:1600018

[14] Kulbak M, Gupta S, Levine I, Hodes G, Cahen D. Cesium enhances long-term stability of lead bromide perovskite based solar cells. Journal of Physical Chemistry Letters. 2016;**7**:167-172

[15] Huang H, Polavarapu L, Sichert JA, Susha A, Urban A, Rogach A. Colloidal lead halide perovskite nanocrystals: Synthesis, optical properties and applications. NPG Asia Materials. 2016;**8**:e328

[16] Di D, Musselman K, Li G, Sadhanala A, Levskaya Y, Song Q, Tan Z, Lai M, Driscoll J, Greenham N, Friend RH. Size-dependent photon emission from organometal halide perovskite nanocrystals embedded in an organic matrix. Nano Letters. 2015;**6**:446-450

[17] Schmidt L, Pertegas A, Carrero S, Malinkiewicz O, Agouram S, Espallargas M, Bolink H, Galian R, Perez-Prieto J. Nontemplate synthesis of $CH_3NH_3PbBr_3$ perovskite nanoparticles. Journal of the American Chemical Society. 2014;**136**:850-853

[18] Gonzalez S, Galian R, Perez-Prieto J. Maximum the emissive properties of $CH_3NH_3PbBr_3$ perovskite nanoparticles. Journal of Materials Chemistry A. 2015;**3**:9187-9193

[19] Li X, Wu Y, Zhang S, Cai B, Gu Y, Song J, Zeng H. $CsPbX_3$ quantum dots for lighting and displays: Room-temperature synthesis, photoluminescence superiorities, underlying origins and white light-emitting diodes. Advanced Functional Materials. 2016;**26**:2435-2445

[20] Huang H, Zhao F, Liu L, Zhang F, Wu X, Shi L, Zou B, Pei Q, Zhong H. Emulsion synthesis of size-tunable $CH_3NH_3PbBr_3$ quantum dots: An alternative route toward efficient light-emitting diodes. ACS Applied Materials and Interfaces. 2015;**7**:28128-28133

[21] Luo B, Pu Y, Yang Y, Lindley S, Abdelmageed G, Ashry H, Li Y, Li X, Zhang J. Synthesis, optical properties, and exciton dynamics of organolead bromide perovskite nanocrystals. Journal of Physical Chemistry C. 2015;**119**:26672-26682

[22] Zhang F, Zhong H, Chen C, Wu X, Hu X, Huang H, Han J, Zou B, Dong Y. Brightly luminescent and color-tunable colloidal $CH_3NH_3PbBr_3$ (X = Br, I, Cl) quantum dots: Potential alternatives for display technology. ACS Nano. 2015;**9**:4533-4542

[23] Protesescu L, Yakunin S, Bodnarchuk M, Krieg F, Caputo R, Hendon C, Yang R, Walsh A, Kovalenko MV. Nanocrystals of cesium lead halide perovskites ($CsPbBr_3$, X = Cl, Br, and I): Novel optoelectronic materials showing bright emission with wide color gamut. Nano Letters. 2015;**15**:3692-3696

[24] Jang D, Park K, Kim D, Park J, Shaojaei F, Kang H, Ahn J, Lee J, Song J. Reversible halide exchange reaction of organometal trihalide perovskite colloidal nanocrystals for full-range band gap tuning. Nano Letters. 2015;**15**:5191-5199

[25] Wong A, Lai M, Eaton S, Yu Y, Lin E, Dou L, Fu A, Yang P. Growth and anion exchange conversion of $CH_3NH_3PbX_3$ nanorod arrays for light-emitting diodes. Nano Letters. 2015;**15**:5519-5524

[26] Nedelcu G, Protesescu L, Yakunin S, Bodnarchuk M, Grotevent M, Kovalenko M. Fast anion-exchange in highly luminescent nanocrystals of cesium lead halide perovskites ($CsPbX_3$, X = Cl, Br, I). Nano Letters. 2015;**15**:5635-5640

[27] Akkerman Q, D'Innocenzo V, Accornero S, Scarpellini A, Petrozza A, Prato M, Manna L. Tuning the optical properties of cesium lead halide perovskite nanocrystals by anion exchange reactions. Journal of the American Chemical Society. 2015;**137**:10276-10281

[28] He H, Yu Q, Li H, Li J, Si J, Jin Y, Wang N, Wang J, He J, Wang X, Zhang Y, Ye Z. Exciton localization in solution-processed organolead trihalide perovskites. Nature Communication. 2015;**7**:10896

[29] Even J, Pedesseau L, Katan C. Analysis of multivalley and multibandgap absorption and enhancement of free carriers related to exciton screening in hybrid perovskites. Journal of Physical Chemistry C. 2014;**118**:11566-11572

[30] Shi Z, Li Y, Zhang Y, Chen Y, Li X, Wu D, Xu T, Shan C, Du G. High-efficiency and air-stable perovskite quantum dots light-emitting diodes with an all-inorganic heterostructure. Nano Letters. 2017;**17**:313-321

[31] D'Innocenzo V, Grancini G, Alcocer M, Kandada A, Stranks S, Lee M, Lanzani G, Snaith H, Petrozza A. Exciton *versus* free charges in organo-lead tri-halide perovskites. Nature Communication. 2014;**5**:3586-3591.

[32] Bekenstein Y, Koscher B, Eaton S, Yang P, Alivisatos A. Highly luminescent colloidal nanoplates of perovskite cesium lead halide and their oriented assemblies. Journal of the American Chemical Society. 2015;**137**:16008-16011

[33] Tan Z, Moghaddam R, Lai M, Docampo P, Higler R, Deschler F, Price M, Sadhanala A, Pazos L, Credgington D, Hanusch F, Bein T, Snaith H, Friend R. Bright light-emitting diodes based on organometal halide perovskite. Nature Nanotechnology. 2014;**9**:687-692

[34] Sutherland B, Sargent E. Perovskite photonic sources. Nature Photonics. 2016;**10**:295-302

[35] Zhang X, Lin H, Huang H, Reckmeier C, Zhang Y, Choy W, Rogach A. Enhancing the brightness of cesium lead halide perovskite nanocrystal based green Light-Emitting Devices through the interface engineering with perfluorinated ionomer. Nano Letters. 2016;**16**:1415-1420

[36] Zhang X, Xu B, Zhang JB, Gao Y, Zheng Y, Wang K, Sun X. All-inorganic perovskite nanocrystals for high-efficiency light-emitting diodes: Dual-phase $CsPbBr_3$-$CsPb_2Br_5$ composites. Advanced Functional Materials. 2016;**26**:4595-4600

[37] Pan J, Sarmah S, Murali B, Dursun I, Peng W, Parida M, Liu J, Sinatra L, Alyami N, Zhao C, Alarousu E, Ng TK, Ooi B, Bakr O, Mohammed O. Air-stable surface-passivated perovskite quantum dots for ultra-robust, single- and two-photon-induced amplified spontaneous emission. Journal of Physical Chemistry Letters. 2015;**6**:5027-5033

[38] Li J, Xu L, Wang T, Song J, Chen J, Xue J, Dong Y, Cai B, Shan Q, Han B, Zeng H. 50-fold EQE improvement up to 6.27% of solution-processed all-inorganic perovskite $CsPbBr_3$ QLEDs via surface ligand density control. Advanced Materials. 2017;**29**:1603885

IntechOpen